AEROSPACE REPORT NO.
TR-2007(8570)-1

HEO Satellite Surface and Frame Charging and SCATHA Low-Level Frame Charging

15 November 2007

Joseph F. Fennell and James L. Roeder
Space Science Applications Laboratory
Physical Sciences Laboratories

Prepared for

Space and Missile Systems Center
Air Force Space Command
483 N. Aviation Blvd.
El Segundo, CA 90245-2808

Authorized by: Engineering and Technology Group

THE AEROSPACE CORPORATION
EL SEGUNDO, CALIFORNIA

This report was submitted by The Aerospace Corporation, El Segundo, CA 90245-4691, under Contract No. FA8802-04-C-0001 with the Space and Missile Systems Center, 483 N. Aviation Blvd., El Segundo, CA 90245. It was reviewed and approved for The Aerospace Corporation by J. A. Hackwell, Principal Director, Space Science Applications Laboratory; and D. C. Marvin, Principal Director, Research and Program Development Office. Michael Zambrana was the project officer for the Mission-Oriented Investigation and Experimentation (MOIE) program.

This report has been reviewed by the Public Affairs Office (PAS) and is releasable to the National Technical Information Service (NTIS). At NTIS, it will be available to the general public, including foreign nationals.

This technical report has been reviewed and is approved for publication. Publication of this report does not constitute Air Force approval of the report's findings or conclusions. It is published only for the exchange and stimulation of ideas.

Michael Zambrana
SMC/EA

REPORT DOCUMENTATION PAGE

Form Approved
OMB No. 0704-0188

1. REPORT DATE (*DD-MM-YYYY*)	2. REPORT TYPE	3. DATES COVERED *(From - To)*
15-11-2007		

4. TITLE AND SUBTITLE

HEO Satellite Surface and Frame Charging
and SCATHA Low-Level Frame Charging

5a. CONTRACT NUMBER
FA8802-04-C-0001

5b. GRANT NUMBER

5c. PROGRAM ELEMENT NUMBER

6. AUTHOR(S)

Joseph F. Fennell and James L. Roeder

5d. PROJECT NUMBER

5e. TASK NUMBER

5f. WORK UNIT NUMBER

7. PERFORMING ORGANIZATION NAME(S) AND ADDRESS(ES)

The Aerospace Corporation
Physical Sciences Laboratories
El Segundo, CA 90245-4691

8. PERFORMING ORGANIZATION REPORT NUMBER

TR-2007(8570)-1

9. SPONSORING / MONITORING AGENCY NAME(S) AND ADDRESS(ES)

Space and Missile Systems Center
Air Force Space Command
483 N. Aviation Blvd.
El Segundo, CA 90245

10. SPONSOR/MONITOR'S ACRONYM(S)
SMC

11. SPONSOR/MONITOR'S REPORT NUMBER(S)

12. DISTRIBUTION/AVAILABILITY STATEMENT

Approved for public release; distribution unlimited.

13. SUPPLEMENTARY NOTES

14. ABSTRACT

In this report, we show the results of spacecraft frame and differential potentials that have been measured over several years on a highly elliptical orbit, HEO2, satellite. The measurements are of charging levels ≤ –30 V, and are summarized according to their occurrence in MLT and L. The data show that the HEO2 satellite frame charged to potentials ≤ –30 V, and that the occurrence of satellite frame charging at these high latitudes mimics the charging local time patterns observed by geosynchronous satellites. In addition, the data show that such charging extends from at least a minimum L ≤ 4 Re to L > 10 Re. About 930 extended frame-charging intervals were observed during the late 1995 through mid-2002 interval. For each charging interval that occurred, the maximum frame voltage and the minimum and maximum L values during charging were obtained. Signatures of differential charging were also observed and are given as a function of L, local time, and charging levels. It was found that the differential charging potential usually exceeded the frame potential and could be estimated by $V_D \sim 74 + 1.384\ V_F$.

15. SUBJECT TERMS

Charging, High Earth orbit, Spacecraft charging

16. SECURITY CLASSIFICATION OF:			17. LIMITATION OF ABSTRACT	18. NUMBER OF PAGES	19a. NAME OF RESPONSIBLE PERSON
					Joe Fennell
a. REPORT	b. ABSTRACT	c. THIS PAGE			19b. TELEPHONE NUMBER *(include area code)*
UNCLASSIFIED	UNCLASSIFIED	UNCLASSIFIED		16	(310)336-7075

Standard Form 298 (Rev. 8-98)
Prescribed by ANSI Std. 239.18

Acknowledgements

This work was supported, in part, under The Aerospace Corporation's Mission-Oriented Investigation and Experimentation and Internal Research and Development programs, funded by the U.S. Air Force Space and Missile Systems Center under Contract No. FA8802-04-C-0001

Contents

Figures

Table

1. Introduction

The issue of spacecraft charging has been of grave concern since the early 1970's and extending to the present (see proceedings of previous Spacecraft Charging Technology Conferences). Numerous anomalies and some loss of spacecraft missions have been ascribed to this phenomena (see Leach and Alexander, 1995 [1]; Spence, et al., 1993 [2]; Koons et al., 1999 [3]; Koons and Fennell, 2006 [4], and references therein). Throughout all the studies of satellite charging, the actual observations of the phenomena have been dominated by data taken in geosynchronous (GEO) and near-geosynchronous orbits and low polar (LPO) orbits. Very few observations have been made at equatorial altitudes below about 5.3 Re or in high polar orbits. Much of the surface charging has been identified using the fact that a satellite's frame develops a negative potential relative to the plasma, and this imposes a characteristic signature in the plasma ion spectra caused by the ions being accelerated to the charged satellite because of its negative potential relative to the ambient plasma. Some observations of differential charging were obtained from dedicated environmental interaction missions such as SCATHA (Stevens and Vampola, 1978 [5]; Fennell, 1982 [6]) and CRRES (Rubin, et al, 1995 [7]).

The charging environment experienced at the magnetic equator maps to higher latitudes in the geomagnetic field. Energetic electron (1–30 keV) angular distributions in the plasma generally have angular distributions that peak at 90° pitch angle near the magnetic equator. These electron intensities fall off for electrons mirroring away from the equator. During substorms, the hot plasma injected into the inner magnetosphere from the nightside plasma sheet is more isotropic than during quiet times. Thus, under substorm conditions, the electron fluxes observed away from the magnetic equator by a satellite in an inclined but high-altitude orbit would experience electron fluxes very similar to those observed by near-equatorial-orbit satellites. One would expect that if the substorm-injected plasmas cause charging of satellites in the middle- to high-altitude equatorial regions that high-altitude inclined orbit satellites, on field lines that map to the equatorial charging regions, would themselves experience charging. Similarly, if highly inclined high-altitude satellites experience charging, one would expect equatorial-orbiting satellites on the same field lines would also experience the charging environment. Thus, charging data from satellites in high-altitude inclined orbits can be used to identify regions with surface charging environments that extend from well below to well above GEO altitude where most of the earlier charging observations were made. Using such an argument, Spence et al. [2] mapped anomalies from a high inclination orbit and showed that the local time and L distribution mirrored the charging occurrences from near-geosynchronous satellites. In this manner, they concluded that the anomalies were caused by satellite surface charging and resultant electrostatic discharges.

This page intentionally blank.

2. Data Sources

2.1 HEO2 Data

In this report, we detail observations from a satellite in a HEO (High-altitude highly inclined Earth Orbit) orbit (Blake et al. 1997 [8]; Grande et al., 1997 [9] and Fennell et al., 2005 [10]). The satellite is designated 1995-034, which we will refer to as HEO2. The HEO2 orbit has a ~7.2 Re geocentric apogee; a low (700–1200 km altitude) perigee, and its orbit inclination is ~63°. The satellite carried a cylindrical plasma analyzer similar to those flown on SCATHA (Fennell, 1982 [6]). The HEO2 plasma analyzer measured, simultaneously, electrons of 25 eV–30 keV and protons of 20 eV–25 keV in 24 logarithmically spaced energy channels. The plasma sensor had a metal planer surface that extended 12 in. in all directions from its aperture and was grounded to the satellite frame. The data from these measurements were available for nearly every orbit for the mid 1995 through 2001 period. The data was taken with a real-time data system that routinely provided data for altitudes corresponding to the range of $L \geq 3.75\ R_E$ (L was calculated using an IGRF field model.) The typical spatial coverage for HEO2 is shown in Figure 1. The orbital period is ~12 h and the apogee of HEO2 generally occurs at fixed longitudes 180° apart. This means there are two regions of orbital coverage at two different ranges of magnetic latitude (thus different L versus magnetic latitude profiles). The two orbits per day for HEO2 are shown as plots of L (black curves) and geocentric radial altitude R

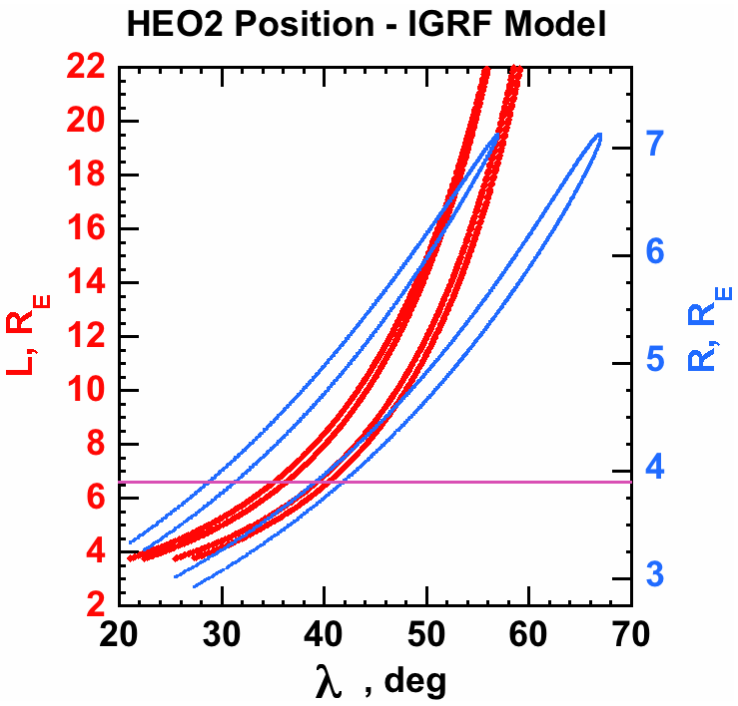

Figure 1. HEO2 orbit plotted as McIllwain L (red) and geocentric radial distance, R (blue), versus magnetic latitude, l.

(gray curves) versus magnetic latitude, λ. We use the data from such L coverage to assess how far above and below geosynchronous (L~6.6) surface charging was observed and to compare the local time extent of the charging to previous determinations.

2.2 SCATHA Data

We used one year (1980) of SCATHA satellite data (Fennell, 1982 [6]; Fennell et al., 1997 [11]) taken from the Goddard Spaceflight Center's SC10 electric fields experiment to estimate SCATHA's frame potential. The SCATHA orbit covers the geocentric altitude range from ~5.3 to ~7.2 R_E, and its less than 24 hour period causes the satellite to drift completely around the Earth in about 70 days. Thus, data are gathered at all SCATHA altitudes in every local time region within a year. Also, the SCATHA orbit had low inclination, and the satellite was oriented with its spin axis lying in the orbit plane. Thus, the "belly band" of the satellite, which was conductive, was always illuminated, except for eclipse periods.

Data derived from the SC10 common mode voltage measurement was used to develop statistics on normal frame charging of SCATHA instead of focusing on the more extreme levels of charging as is usually done. The common mode voltage is measured between the conductive section at the end of a 50-m antenna that is in contact with the plasma and the satellite frame in three separate voltage ranges, ±15, ±300, and ±5000 V. This common mode voltage has been shown to agree with estimates of the SCATHA frame potential obtained from plasma measurements on board (see Mullen, et al., 1986 [12] and Gussenhoven and Mullen, 2000 [13]). While the common mode voltage is not expected to give a precise measure of the frame potential under all conditions, it should provide a reasonable view of the variation of the frame potential on a relative basis. For our study, only data taken when the satellite and antenna were sunlit were used. In addition, the electric-field boom was required to be oriented perpendicular to the satellite sun line to avoid satellite shadow effects. This provided two possible data samples per spin period. We used only one of these samples each spin, which was taken when the antenna tip was pointed approximately parallel to ecliptic north.

3. HEO2 Frame and Differential Charging Observations

The HEO2 plasma data were plotted as electron and proton energy-time spectrograms as shown in Figure 2. The ion energy scale (lower panel) in Figure 2 is inverted relative to the electron energy scale (upper panel) so the ion energy increases downward. The electron and ion flux scales are gray-scale coded as indicated on the gray-scale bar on the right. The spectrograms were visually examined for charging signatures. Figure 2 contains both a frame charging signature (in the ion spectrogram) and a differential charging signature (in the electron spectrogram), as noted by the arrows on the figure. The frame potential (hereafter designated V_F) is evidenced by the acceleration of ions to the satellite, giving rise to a intense flux of ions at an energy corresponding to the frame potential relative to the space plasma. The ion spectrogram in Figure 2 indicates that the HEO2 satellite frame was already charged to about −1 kV at the time of the first data accessible for this orbit on 5 May 1998. HEO2 was moving outward towards apogee starting at L~5.2 R_E near MLT~3.3 h and $\lambda \geq 30°$. As the satellite moved to larger L and higher altitude, the magnitude of the frame charging slowly decreased to near zero by 1820 UT.

Differential charging is evidenced in the electron distributions in a manner similar to how the signature of frame charging is exhibited in the ion distributions. In Figure 2, the charging signature in the electron spectrogram indicates that a nearby surface was initially charged to ≥–900 V relative to the satellite frame. The bright charging line in the electron spectrogram indicates that cold electrons emitted from the charged surface fall through a potential drop relative to the electron sensor, which is grounded to the satellite frame. Thus, the charged surface that gives rise to the charging signature in

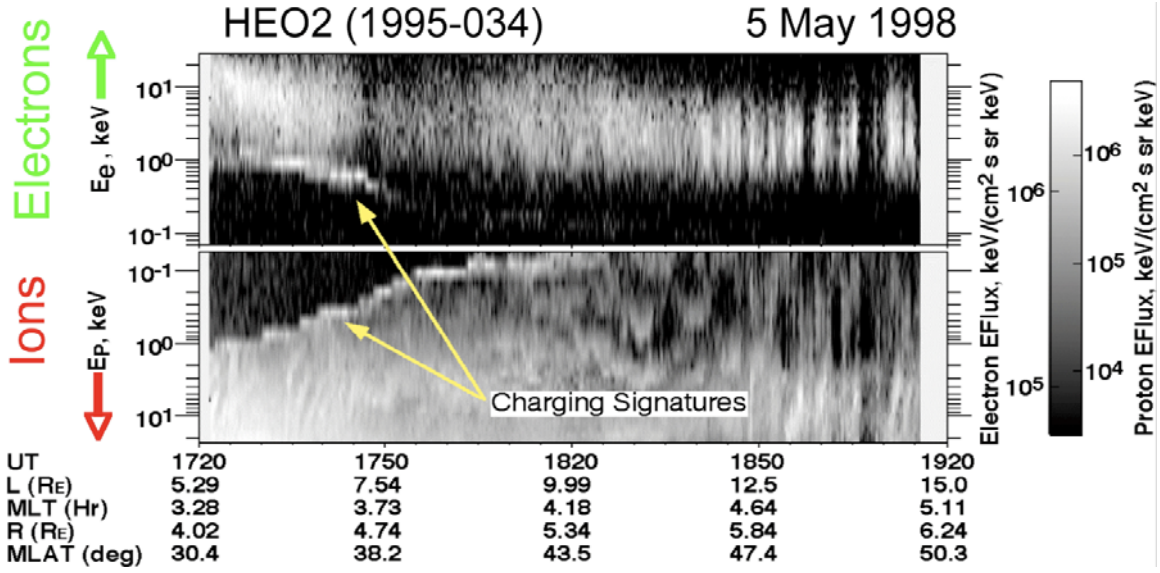

Figure 2. Energy-Time spectrogram of electrons (top panel) and ions (bottom panel) for 5 May 1998. The left-hand ion energy scale is inverted with energy increasing downward. The charging interval is marked.

the electrons is initially at a potential of ~ –1900 V relative to the space plasma and ~ –900 V relative to the HEO2 frame and the plasma analyzer. This differential potential (hereafter denoted V_D) of the charged electron-emitting surface decreased as HEO2 moved to higher L and altitude, just like the frame potential did. This electron charging signature shows that a level of differential charging exists on the satellite. While we suspect that it is a dielectric-coated radiator or some portion of the MLI (multilayer insulation) blanket near the plasma instrument that is charged to a potential V_D and is the source of either photo or secondary electrons that arrive at the plasma sensor with energy ~ V_D, creating the differential charging signature of Figure 2. However, we cannot uniquely identify the electron-emitting source from these data.

The maximum and minimum L values, MLT (magnetic local time), and maximum potential was obtained for each traversal through the radiation belts wherein the HEO2 frame and differential charging were observed. There were 930 such intervals for the frame charging, and their L and MLT distributions are shown in Figure 3. The minimum L (hereafter denoted L_{MIN}) where charging was observed during a traversal is indicated by the diamond symbols in Figure 3. The circle symbols indicate the corresponding maximum L (hereafter denoted L_{MAX}). The position of geosynchronous orbit is indicated by dashed line in Figure 3 for reference. It is clear that the local time distribution of the points is much like the local-time charging probability distributions observed by geosynchronous satellites from different sources. However, the HEO2 results clearly show that the frame charging extended to much higher and lower L values than geosynchronous. It also shows that there is a trend for the HEO2 frame charging to occur at larger L in the pre-noon sector than in the post-midnight

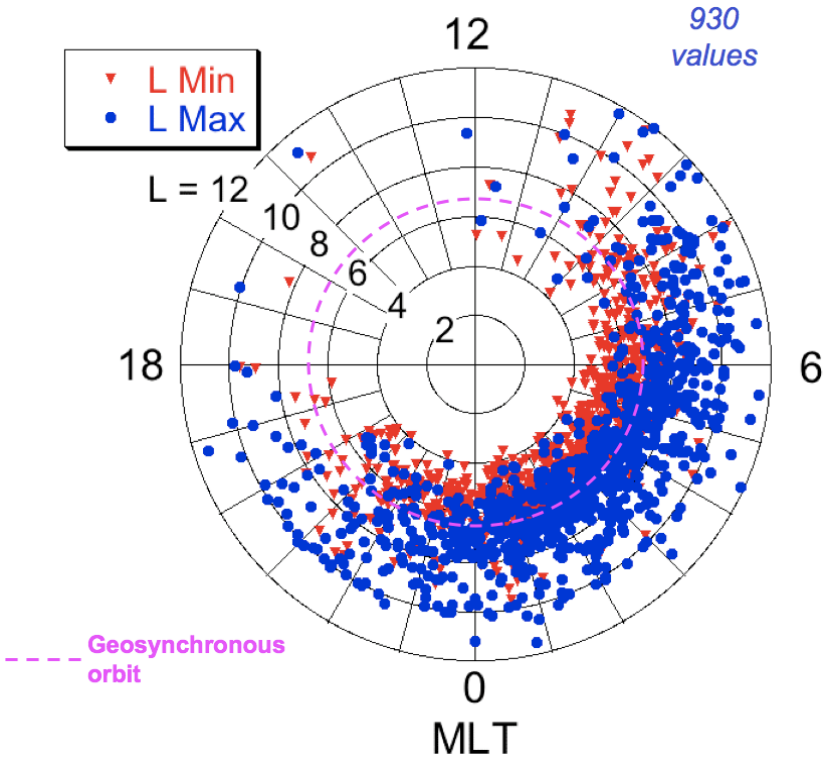

Figure 3. L versus MLT distribution of the minimum L (red diamonds) and the maximum L (blue circles) at which frame charging was observed by the HEO2 satellite. See text for details.

sector. Figure 3 also shows that the HEO2 satellite frame occasionally, but rarely, charged in the 9–20 MLT region, i.e., from pre-noon on the dayside to post dusk. The bulk of the HEO2 frame charging occurred from pre-midnight through post-dawn local times.

Figure 4 shows a similar result for the differential charging on HEO2. There are fewer data points because of a problem with the plasma electron sensor that limited its ability to show the differential charging line at later times. However, Figure 4 shows that the L-MLT distribution for the differential charging, given the limited number of samples, is essentially the same as for the frame charging. Again, the L_{MIN} of the differential charging extends well below the geosynchronous L value, and the L_{MAX} extends well above, just like in Figure 3. We should note here, that the fact that the L_{MAX} does not extend much below L = 4 is partially a bias introduced by the real-time data coverage (see Figure 1 and below).

If the data in Figures 3 and 4 are binned in L independent of MLT, one obtains the L dependence of the charging as shown in Figure 5. This figure shows the probability of observing HEO2 frame and differential charging peaks in the L = 5.5–7 range, near geosynchronous L. Each vertical bar corresponds to a spatial resolution of $\Delta L = 0.5$ Re and $\Delta L = 1$ for the HEO2 frame charging and the differential charging, respectively. For the L_{Max} distributions, the charging occurrence is low for $L_{Max} < 5$ and $L_{Max} > 10.5–11$. Similarly, for the L_{Min} distributions, the charging occurrence is low for $L_{Min} < 4.5$ and $L_{Min} > 7.5–8$. Thus, the HEO2 charging occurs predominantly in the $4.5 < L < 11$ region. This is consistent with the L regions where the inner plasma sheet hot electron population

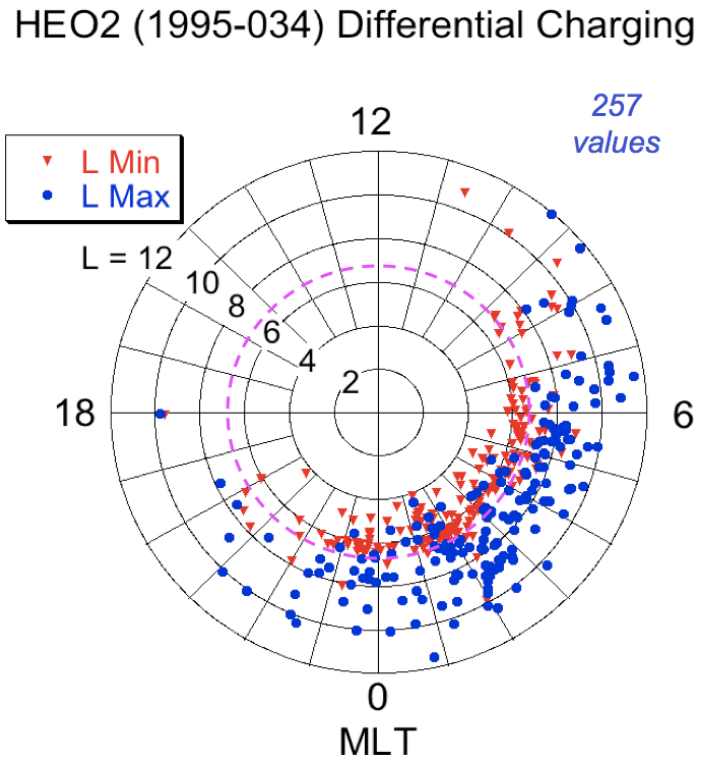

Figure 4. Like Figure 3 except for the differential charging signatures observed in the electron spectrograms.

exists during and following substorms. Table 1 provides a summary of the data in Figure 5. As noted above, the lower L charging may be under represented in these data because of the low-L limits of the data acquisition. We have not been able to normalize these data relative to time spent in each region as yet. This is being done, but was not ready in time for this publication. However, the decrease in relative occurrence of charging between L = 6 and L = 5 is real and not constrained by the data coverage in L.

Table 1. Statistics on L Values of Charging

Frame Charging					
	Ave	**Median**	**Min**	**Max**	**SD**
L_{MAX}	7.72	7.41	4.14	15.45	1.75
L_{MIN}	6.09	5.84	3.61	12.50	1.23
Differential Charging					
	Ave	**Median**	**Min**	**Max**	**SD**
L_{MAX}	8.32	8.00	4.38	14.22	1.75
L_{MIN}	6.39	6.27	4.07	10.80	1.08

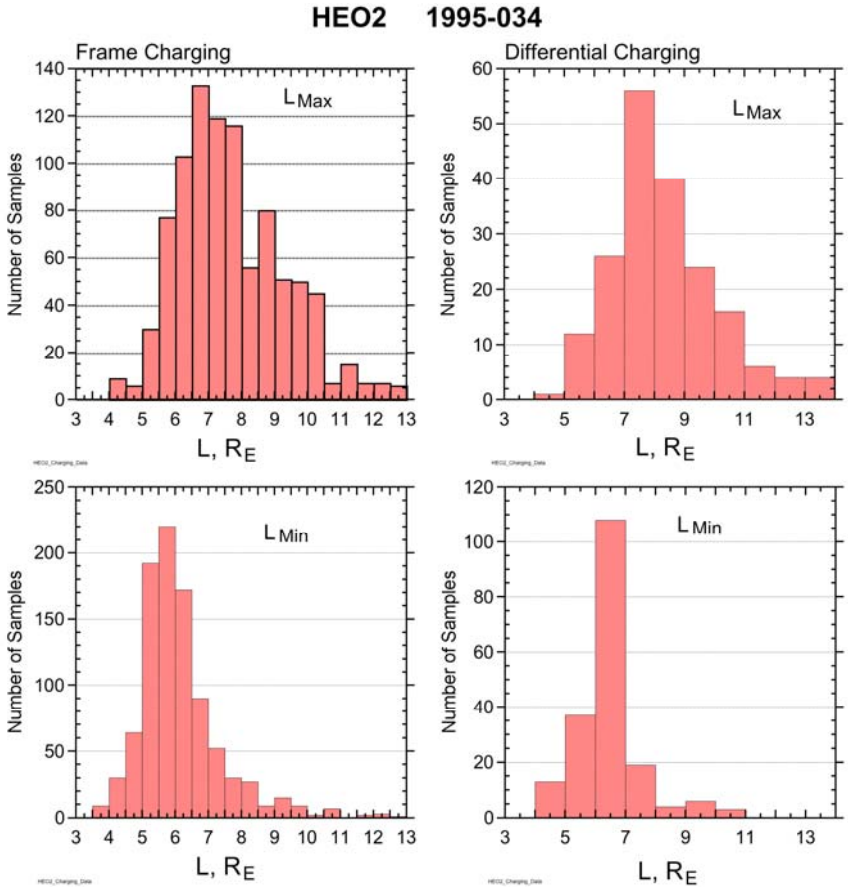

Figure 5. L distributions of frame charging (left panels) and differential charging (right panels) observed by HEO2.

If the data in Figures 3 and 4 are binned in MLT bins independent of L, one obtains the MLT distribution of frame and differential charging for L_{MAX} and L_{MIN} as shown in Figure 6. Each vertical bar in Figure 2 represents two hours of local time. The MLT distribution of HEO2 frame charging is very much the same as that found for geosynchronous orbit measurements in the past (see Koons et al. 2005 [14] and references therein). The L_{MIN} and L_{MAX} MLT distributions of HEO2 frame charging (left panels in Figure 6) are the same with essentially no frame charging observed in the 12 to 18 MLT region. The MLT distributions of HEO2 differential charging (right panels) are nearly identical to that of the frame charging. For both types of charging, their maximum occurrence is in the post-midnight region (00–08 MLT). This indicates that whenever charging occurs, it shows the same local time preference roughly independent of the L value where it occurs. This can be seen in Figures 3 and 4.

Since we simultaneously have the differential and frame charging, we can test to see whether there is a relationship between the levels of HEO2 frame and differential charging potentials. This can pro vide a clue as to how sensitive the levels of charging are to the materials involved. Figure 7 shows

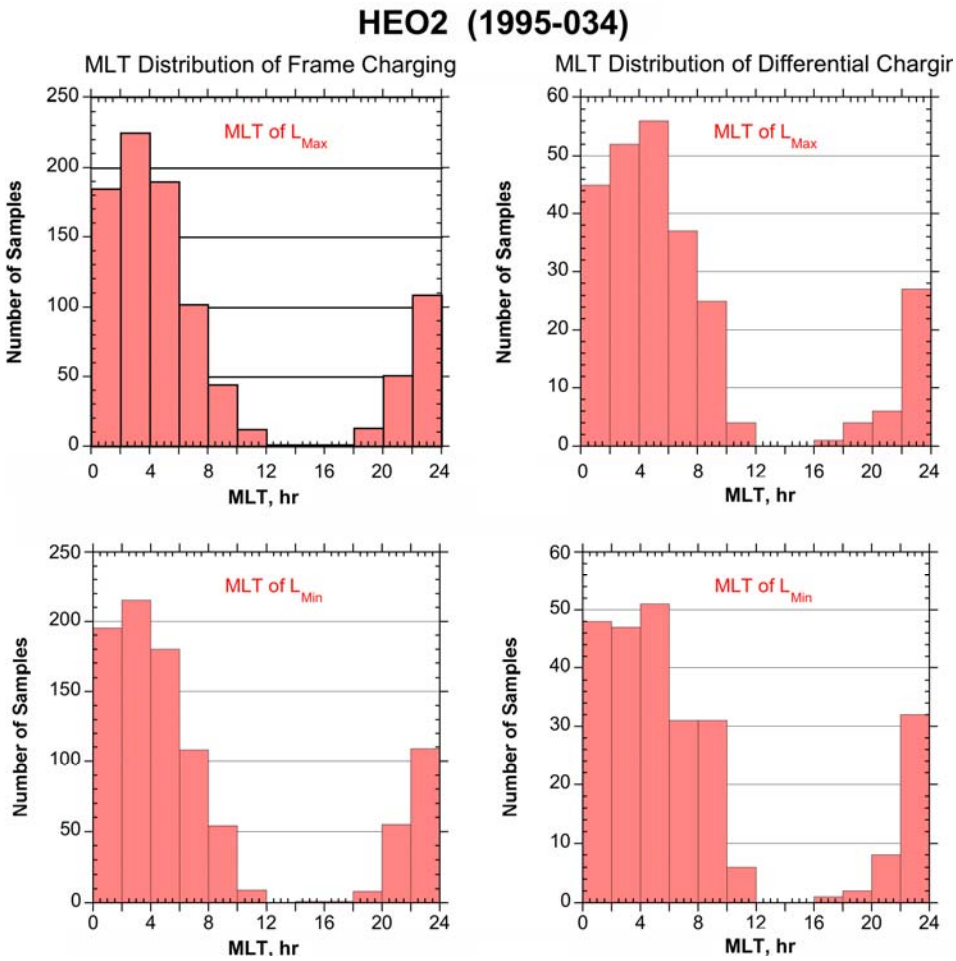

Figure 6. MLT Distribution of HEO2 frame charging (left panels) and differential charging (right panels) for L_{MAX} (upper panels) and L_{MIN} (lower panels).

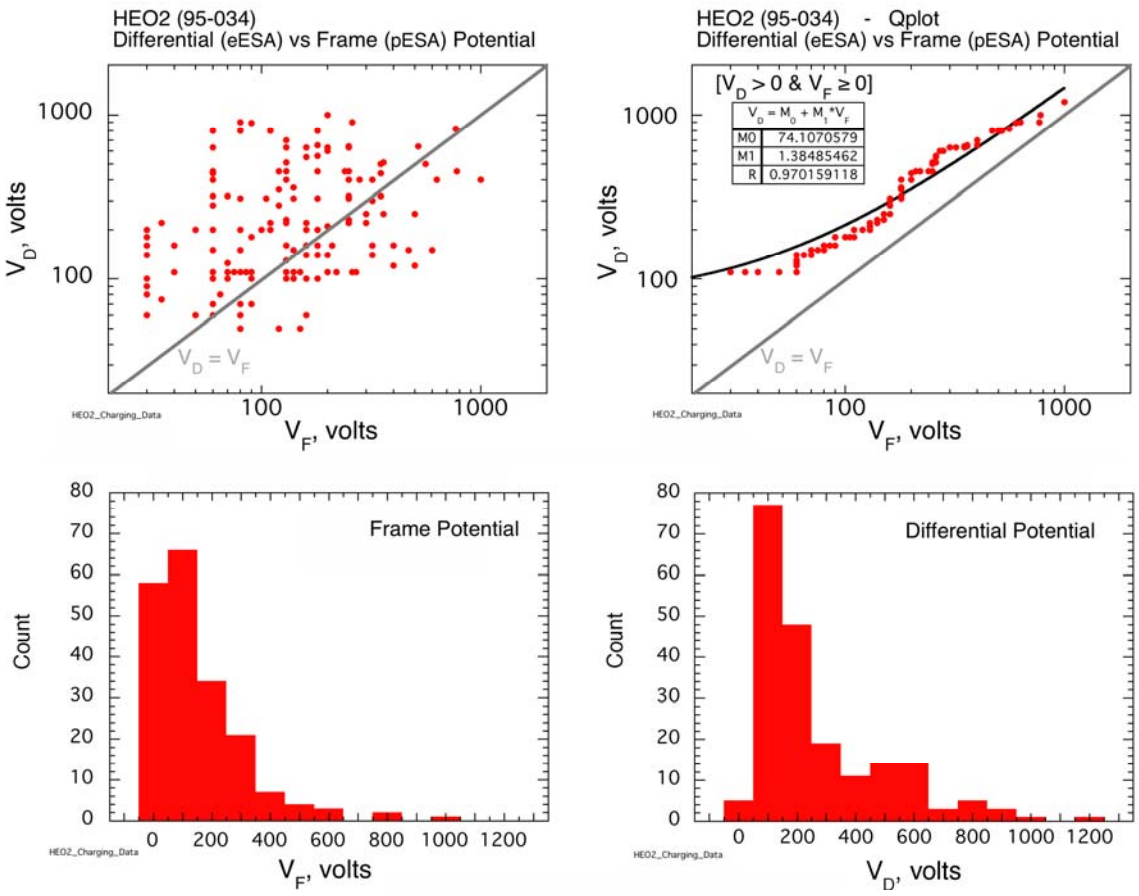

Figure 7. Distributions of HEO2 frame and differential potentials (bottom panels), the relationship between the differential and corresponding frame potential (top left panel) and the Qplot derived from the ordered data.

four data panels that relate the HEO2 differential potential to the frame potential (upper left), the distributions of the potentials (bottom panels), and a Qplot (upper right) showing the linkage between the differential potentials and the frame potentials observed. The top panels in Figure 7 show that there is a clear relationship between the HEO2 differential and frame potentials. These plots also strongly indicate that for HEO2 the differential potential, V_D, was usually larger than the frame potential, V_F. The Qplot is derived from the ordered distributions for the simultaneous frame and differential potentials (not shown here). As the fit to the Qplot data shows, V_D can be reasonably related to V_F as: $V_D \sim 74 + 1.385\ V_F$.

4. SCATHA Observations of Low-Level Charging

As noted above, we examined all SC10 common mode voltage data from 1980 to get a picture of what normal charging conditions are for a near-geosynchronous spacecraft such as SCATHA. This effort was stimulated by concern that satellites could have low negative potentials for significant fractions of their time on orbit. If this were true, one would have to account for such charging when modeling possible attraction of outgassed contaminants back to a spacecraft when the contaminant molecules are photo or impact ionized while still within the satellite's plasma sheath. The plasma sheath thickness, or Debye length, can be meters at geosynchronous altitudes because of the relatively high plasma electron temperature and the relatively low density that occurs there at SCATHA altitudes, especially in the nightside regions. Thus, it seemed that conditions could be favorable for charging-enhanced attraction of outgassed contaminants, especially if the vehicles were charged negatively a significant fraction of the time.

The focus of this study was not on the high levels of charging that lead to electrostatic discharges but on what was the normal charging history for a near-geosynchronous satellite on a day-to-day basis. To this end, we collected a satellite frame potential estimate from the SC10 experiments common mode voltage values every minute for a year. As noted above, this provided a good sampling of data from all SCATHA altitudes at all local times.

Figure 8 shows the results of this short study. Figure 8a shows the probability of occurrence of frame charging levels based on the ±15-V range of the SC10 common mode measurement for the full year. The roll-off at $V_F < -14$ V is an artifact of saturation when the voltage reached or exceeded the ±15-V

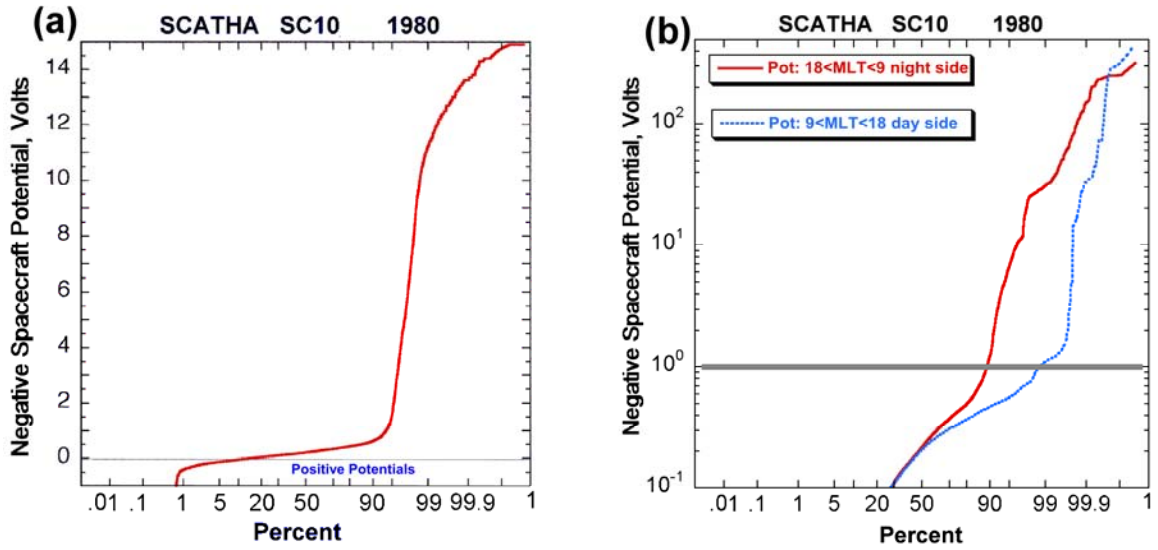

Figure 8. Occurrence probability of SCATHA frame potentials: (a) $V_F > -15$V for 1980; (b) $V_F > -400$V for 1980 on the dayside (blue) and nightside (red) of the inner magnetosphere.

range. The positive V_F values are suppressed in Figure 8a. Nevertheless, from Figure 8a, we can infer that the SCATHA frame was positive relative to the SC10 antenna tip about 10% of the time. Figure 8a also shows that $V_F > -1$ V about 94% of the time. Thus, $0 \geq V_F \geq -1$ V about 84% of the time. It also shows that the distribution of $V_F < -1$ V increased rapidly in the last 5% of the data samples. It is amongst these last 5% of the data that the large negative V_F values associated with electrostatic discharges would occur.

Figure 8b shows the probability of negative frame charging on SCATHA for two separate local time regions. These are the nightside (red curve) and the dayside (blue dotted curve) of the magnetosphere. We chose to separate the data as shown since we expected the largest negative frame charging should occur in the pre-midnight through post-dawn regions as earlier studies and the HEO2 results, above, had shown. For Figure 8b, we combined the data from all ranges of the SC10 common mode voltage measurement, but limited the plot to values in the range 0 to ±400 V. The figure clearly shows that about 10% of the time $V_F < -1$ V on the nightside while only ~1% of the time is $V_F < -1$ V on the dayside. The figure also shows that $V_F > -0.25$ was equally probable in both local time regions and that 30% of the time $V_F > -0.1$ V. So, much like large negative V_F potentials, the low negative V_F potentials are predominant on the nightside at near geosynchronous altitudes.

5. Discussions and Conclusions

We have shown that satellites traversing regions that map magnetically in MLT to near-geosynchronous equatorial MLT regions where surface charging occurs will experience surface and frame charging in the same manner as equatorial satellites. This validates the assumption that the charging environment extends along magnetic field lines to high latitudes. This had been previously borne out by the fact that satellites are known to charge, even at low altitudes, in the auroral regions. However, the auroral charging process is complicated by the generally high background density of the ionospheric plasma, the auroral acceleration processes, and the fact that low-altitude satellites may often be in Earth's shadow (Anderson and Koons, 1996 [15]; Anderson, 2000 [16]; Eriksson and Wahlund, 2005[17]; Gussenhoven et al., 1985 [18[). In addition, low-altitude satellites generate ram and wake regions in the cold background ions because of the satellite's high velocity compared to that of the cold ions.

Unfettered by such issues, satellites in high-altitude, low- to high-inclination orbits should experience surface and frame charging whenever they are in the hot plasma sheet environment. This is indeed what the HEO2 data show. HEO2's surface and frame charging occurs from well below to well above geosynchronous L values. One would expect that such charging occurs when the electron temperature is high enough and the hot electron density is large enough to cause the charging, even in sunlight. It is no surprise then that such regions extend from below to above geosynchronous in the pre-midnight to post-dawn regions of the inner magnetosphere. This is consistent with the fact that the inner edge of the nightside plasma sheet extends down to altitudes that are within 1 Re or so of the plasmasphere boundary. During active periods, such as during substorms and magnetic storms, the plasmasphere is eroded and the plasma sheet penetrates to lower L. It is during substorms that one generally experiences high levels of satellite charging at geosynchronous orbit. It should also be true for satellites at higher latitudes and on similar L values. In reverse, the fact that HEO2 experiences high levels of charging, well off the magnetic equator, over a wide range of L values means that equatorial satellites should also experience charging over the same range of L. This has been partially borne out, at least below geosynchronous altitudes, by CRRES observations of frame charging (Rubin et al., 1995 [7]).

The HEO2 data showed that differential charging occurred in the same regions as did the frame charging, much like similar observations made by the SCATHA and Intelsat Spacecraft (Gussenhoven et al., 2000 [13]; Fennell, et al., 2002 [19]; Koons et al., 2005 [20]). In the HEO2 case, the material being differentially charged cannot be conclusively identified. However, based on the materials that were in the neighborhood of the plasma sensor used to detect the charging, it was most likely the Kapton outer layer of multilayer insulation or a silver-Teflon-coated radiator. Statistically, the material tended to charge to higher levels relative to the frame than the HEO2 frame did relative to the space plasma.

Examination of the SCATHA satellite frame potential every minute for a year showed that about 90% of the time its frame potential was negative, but most of that time (~84%) the potentials were no more

than a volt or so. The analysis reinforced the fact that the most negative frame voltages were observed in the nightside magnetosphere. The frame potential was > –1 V ~90% of the time on the nightside and ~99% of the time on the dayside. So, even for quite low negative potentials, the occurrence is greatest on the nightside. Nevertheless, if low negative voltages (>–1 V) are sufficient to attract escaping outgassed molecules that are ionized within the first few meters of a satellite, then these potential distributions have to be considered when estimating satellite self-contamination because they occur for a significant percentage of the time, in near-geostationary orbit.

References

1. Leach, R. D. and M. B. Alexander, "Failures and anomalies attributed to spacecraft charging," NASA Reference Publication 1375, August 1995, (available from National Aeronautics and Space Administration, Marshall Space Flight Center, MSFC, Alabama 35812 USA), p. 16.

2. Spence, H. E., J. B. Blake, and J. F. Fennell, "Surface charging analysis of high-inclination, high-altitude spacecraft: identification and physics of the plasma source region," *IEEE Transactions on Nuclear Science*, **40**(6), pp. 1521–1524, 1993.

3. Koons, H. C., J. E. Mazur, R. S. Selesnick, J. B. Blake, J. F. Fennell, J. L. Roeder, and P. C. Anderson, "The impact of the space environment on space systems," in *Proceedings of the 6th Spacecraft Charging Technology Conference*, November 2–6, 1998, AFRL-VS-TR-20001578, Air Force Research Laboratory, Hanscom, Mass., Sept. 2000; and The Aerospace Corporation, TR-99(1670)-1, July 1999.

4. Koons, H. C. and J. F. Fennell, "Space weather effects on communications satellites," *Radio Sci. Bulletin*, No. 316, p. 27, Mar. 2006.

5. Stevens, J. R. and Vampola, A. L. (eds.), "Description of the Space Test Program P78-2 Spacecraft and Payloads," Space and Missile Systems Organization, Los Angeles, CA, Tech. Rept. SAMSO TR-78-24, 1978.

6. Fennell, J. F., *Description of P78-2 (SCATHA) Satellite and Experiments*, C. T. Russell and D. J. Southwood, eds, American Geophys. Union, 1982.

7. Rubin, A. G., W. J. Burke, and D. A. Hardy, "Low-energy ion spectral peaks detected by CRRES in the plasma sheet," *J. Geophys. Res.*, **100**, 19221, 1995.

8. Blake, J. B., D. N. Baker, N. Turner, K. W. Ogilvie, and R. P. Lepping, "Correlation of changes in the outer-zone relativistic-electron population with upstream solar wind and magnetic field measurements," *Geophys. Res. Lett.*, **24**, 927, 1997.

9. Grande, M., J. Fennell, S. Livi, B. Kellett, C. H. Perry, P. Anderson, J. Roeder, H. Spence, T. Fritz, B. Wilken, "First polar and 95-034 observations of the midaltitude cusp during a persistent northward IMF condition," *Geophys. Res. Lett,* **24***,* 1475–1478, 1997

10. Fennell, J. F., J. B. Blake, R. Friedel, and S. Kanekal, "The Energetic Electron Response to Magnetic Storms: HEO Satellite Observations," in *Physics and Modeling of the Inner Magnetosphere*, AGU monograph 155, p87, 2005.

11. Fennell, J. F., G. M. Boyd, M. T. Redding, and M. C. McNab, "Data recovery from the SCATHA satellite," The Aerospace Corporation, ATR-97(7400)-1, Sep. 1997.

12. Mullen, E. G.; Gussenhoven, M. S.; Hardy, D. A.; Aggson, T. A.; Ledley, B. G.; Whipple, E., "SCATHA survey of high-level spacecraft charging in sunlight," *J. Geophys. Res,* **91**, 1474, 1986.

13. Gussenhoven, M. S. and E. G. Mullen, "SCATHA retrospective: Satellite frame charging and discharging in the near-geosynchronous environment," in *Proceedings 6th Spacecraft Charging Technology Conference*, AFRL-VS-TR- 20001578, 1 September 2000.

14. Koons, H., J. Mazur, A. Lopatin, D. Pitchford, A. Bogorad, and R. Herschitz, "Spatial and temporal correlation of spacecraft surface charging in geosynchronous orbit," *J. Spacecraft and Rockets,* **A11**, October, 2005.

15. Anderson, P. C. and H. C. Koons, "A spacecraft charging anomaly on a DMSP satellite in an aurora," *J. Spacecraft Rockets,* **33**, 734, 1996.

16. Anderson, P. C., "Surface charging in the auroral zone on the DMSP spacecraft in LEO," in *Proceedings of the 6th Spacecraft Charging Technology Conference*, AFRL-VS-TR-20001578, Air Force Research Laboratory, Hanscom, Mass., pp. 55–59, Sep. 2000.

17. Eriksson, A. I. and J.-E. Wahlund, "Charging of a conductive spacecraft in the auroral zone," in *Proceedings of the 9th Spacecraft charging technology conference - 2005*, JAXA-SP-05-001E, April 2005.

18. Gussenhoven, M. S., D. A. Hardy, F. Rich, W. J. Burke, and H.-C. Yeh, "High Level Charging in the Low-Altitude Polar Auroral Environment," *J. Geophys. Res.,* **90**, 11000, 1985.

19. Fennell, J. F., J. L. Roeder, and H. C. Koons, "Substorms and magnetic storms from the satellite charging perspective," in *Space Weather Study Using Multipoint Techniques, Proceedings of the COSPAR Colloquium* (ed Ling-Hsiao Lyu), Taipei, Taiwan, September 27–29, 2000, Pergamon, Amsterdam, pp. 163–173, 2002.

20. Koons, H., J. Mazur, A. Lopatin, D. Pitchford, A. Bogorad, and R. Herschitz, "Spatial and temporal correlation of spacecraft surface charging in geosynchronous orbit," *J. Spacecraft and Rockets,* **A11**, October, 2005.

PHYSICAL SCIENCES LABORATORIES

The Aerospace Corporation functions as an "architect-engineer" for national security programs, specializing in advanced military space systems. The Corporation's Physical Sciences Laboratories support the effective and timely development and operation of national security systems through scientific research and the application of advanced technology. Vital to the success of the Corporation is the technical staff's wide-ranging expertise and its ability to stay abreast of new technological developments and program support issues associated with rapidly evolving space systems. Contributing capabilities are provided by these individual organizations:

Electronics and Photonics Laboratory: Microelectronics, VLSI reliability, failure analysis, solid-state device physics, compound semiconductors, radiation effects, infrared and CCD detector devices, data storage and display technologies; lasers and electro-optics, solid-state laser design, micro-optics, optical communications, and fiber-optic sensors; atomic frequency standards, applied laser spectroscopy, laser chemistry, atmospheric propagation and beam control, LIDAR/LADAR remote sensing; solar cell and array testing and evaluation, battery electrochemistry, battery testing and evaluation.

Space Materials Laboratory: Evaluation and characterizations of new materials and processing techniques: metals, alloys, ceramics, polymers, thin films, and composites; development of advanced deposition processes; nondestructive evaluation, component failure analysis and reliability; structural mechanics, fracture mechanics, and stress corrosion; analysis and evaluation of materials at cryogenic and elevated temperatures; launch vehicle fluid mechanics, heat transfer and flight dynamics; aerothermodynamics; chemical and electric propulsion; environmental chemistry; combustion processes; space environment effects on materials, hardening and vulnerability assessment; contamination, thermal and structural control; lubrication and surface phenomena. Microelectromechanical systems (MEMS) for space applications; laser micromachining; laser-surface physical and chemical interactions; micropropulsion; micro- and nanosatellite mission analysis; intelligent microinstruments for monitoring space and launch system environments.

Space Science Applications Laboratory: Magnetospheric, auroral and cosmic-ray physics, wave-particle interactions, magnetospheric plasma waves; atmospheric and ionospheric physics, density and composition of the upper atmosphere, remote sensing using atmospheric radiation; solar physics, infrared astronomy, infrared signature analysis; infrared surveillance, imaging and remote sensing; multispectral and hyperspectral sensor development; data analysis and algorithm development; applications of multispectral and hyperspectral imagery to defense, civil space, commercial, and environmental missions; effects of solar activity, magnetic storms and nuclear explosions on the Earth's atmosphere, ionosphere and magnetosphere; effects of electromagnetic and particulate radiations on space systems; space instrumentation, design, fabrication and test; environmental chemistry, trace detection; atmospheric chemical reactions, atmospheric optics, light scattering, state-specific chemical reactions, and radiative signatures of missile plumes.